Meccanica (2023) 58:473–492
https://doi.org/10.1007/s11012-022-01538-0

SELF-PROPELLED ROBOTS: FROM THEORY TO APPLICATIONS

Locomotion analysis of self-propelled board by inclined internal mass motion with slider-crank mechanism

Norihiro Kamamichi · Katsuhisa Furuta

Received: 2 November 2021 / Accepted: 6 May 2022 / Published online: 14 June 2022

Abstract This paper presents a self-propelled board which locomotes by the inclined rectilinear reciprocal motion of the internal mass generated by the slider-crank mechanism. The board is named "KF Board"-simplifying Kamamichi-Furuta Board. The Board is assembled by using LEGO components. Simple constant torque applied to the crank disk of the KF board generates the reciprocal motion of the internal mass which makes the board locomote with corresponding gaits. Mathematical simulations of the locomotions are done for the simplified mathematical models of the KF board, and clarifies the relations of the frequency and the inclined angle of the reciprocal motion of the internal mass to the locomotion velocity and the effects of the orbital motion of the internal mass. The internal motion of the internal mass is further studied to have near elliptic orbit by the choice of its position on the connecting rod from the crank to the slider.

Keywords Self-propelled robots · Locomotion · KF board · Friction board · Capsubot · Motion analysis

N. Kamamichi (✉)
Department of Robotics and Mechatronics, Tokyo Denki University, 5 Senju-asahi-cho, Adachi-ku, 120-8551 Tokyo, Japan
e-mail: nkama@mail.dendai.ac.jp

K. Furuta
President Emeritus, Tokyo Denki University, Tokyo, Japan
e-mail: kfuruta@jcom.home.ne.jp

1 Introduction

The machine locomotion is ordinary done by actuating devices such as wheels, legs, propellers and others. Without such devices, the machine locomotion on the resistive surface can also be done by appropriate lateral reciprocal motion of the internal mass, which had been presented in the series of the papers of mechanical snakes by F.L. Chernousko [1, 2]. Similar ideas have been exploited as the impact driving systems [3, 4]. Prof. Chernousko visited and gave seminars to the group of Human Adaptive Mechatronics at Tokyo Denki University. The authors had studied the control of pendulums for a long time [5, 6] and started to study the cart locomotion by swinging the pendulum [7] at his group through the fusion of the ideas.

The cart on passive wheels named "Pendulum-driven cart" was reported firstly in 2005 at the 2nd COE workshop on Human Adaptive Mechatronics at Tokyo Denki University. The pendulum-driven cart shown in Fig. 1 was assembled by using LEGO Mindstorms 2.0 components. It moves forward by quickly swinging the pendulum backward due to the conservation of the momentum, since the friction force on the resistive surface is comparably small against the driving force for the fast forward movement. It stays during the pendulum slowly swinging back forward, since the friction force is large against the driving force for the slow backward movement. The control design of the pendulum swing is difficult

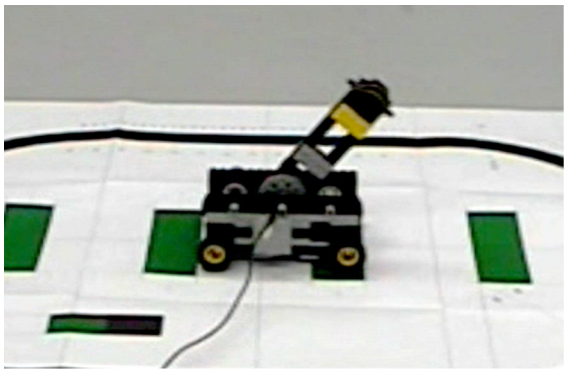

Fig. 1 Pendulum-driven cart presented in [7]

Fig. 2 Capsubot presented in [8]

due to consideration of the effects of the change of the swing direction. The mathematical model was constructed under the assumption that friction force makes the cart stay completely while the pendulum slowly swings forward, and the cart locomotes by the quick swing of the pendulum to backward. Desirable pattern of the pendulum motion was derived theoretically, and the pendulum was controlled to follow the pattern [7].

After the return of Prof. Chernousko, H. Li and K. Furuta had made the capsule type micro robot based on the idea of the cart with a swinging pendulum, that locomotes on the resistive surface by the lateral reciprocal motion of the internal mass [8]. The robot was named "Capsubot" by Prof. Karl J. Astrom who stayed at Tokyo Denki University at those days. The capsubot shown in Fig. 2 was presented at IEEE Conference on Decision and Control(CDC) [8]. The capsubot was proposed to incorporate a camera, a lightning system, a transmitting and receiving device, a control device and a power supply device in a capsule body. The miniaturized capsule was aimed to be used for the examination of the human organ by swallowing it. Prof. Chernousko has presented a survey of the studies in [9].

These systems have two separate masses. One is the reciprocally moving internal mass, such as the pendulum mass and the internal mass of the capsubot, and the other is the main body mass such as the cart with passive wheels and capsule outer body. In [7] [8], the locomotive motion of the pendulum-driven cart and the capsubot were designed to control the internal mass to satisfy the four steps;

Step 1: Large backward acceleration of the internal mass causes the forward acceleration of the main body.
Step 2: Backward deceleration of the internal mass causes deceleration of the main body.
Step 3: Small backward deceleration causes the main body to be stationary.
Step 4: Forward slow motion of the internal mass applied for returning to start position, during the main body remains stationary.

The internal mass of the pendulum-driven cart was the pendulum rotated by the DC motor [7]. The optimization of the pattern and control of the internal mass for the pendulum-driven cart were studied [10] and a cart with double inverted pendulum was also investigated [11]. The internal mass of the capsubot was mainly the permanent magnet driven by the magnetic coils [8]. There had been considerable number of studies on the motion generation and control for the capsubot. Typical motion generation methods were based on acceleration patterns design of the internal mass or optimization utilizing dynamical models [12–15]. Feedback control for the capsubot had been studied through various approaches [16–21]. Further studies had been done by decomposing the above 4th step into three steps for improving the control strategy of the internal mass [22], and by attaching the spring for achieving quick movement of the internal mass of the capsubot [23–25].

The locomotive systems can improve the efficiency by controlling the pressure for the friction. The friction should be made smaller while it moves forward and larger while it stays. The friction force is known to be given by friction coefficient μ times the normal pressure [26]. Therefore, the smaller friction is realized by making the normal pressure smaller, which can be achieved by the acceleration of the internal mass to have downward direction component. Conversely, the larger friction is achieved by the upward

acceleration of the internal mass. This idea was realized by "Friction board with inclined slider" [27], whose photo is shown in Fig. 3. The mathematical model of the friction board was derived and the control algorithm for the motion of the internal mass was given. The developed friction board locomoted satisfactorily with moderate payload. The locomotive motions of the developed systems had been designed based on the four steps described previouly and considered both dynamic and static friction between the cart and floor. The further theoretical studies had been done for the capsubot using the sliding reciprocal motion of the internal mass [28].

In the beginning, sophisticated ideal control system had been difficult to be implemented to make the internal mass of Capsubot and Pendulum-driven cart follow the pre-computed optimal profile for the small-sized system. The small-size capsubot had used the electric coil for internal force actuation by the magnetic fields and could not use a position sensor. So for a small capsubot, the open-loop optimal control should be implemented [8]. The Step 3 was implemented not to collide the internal mass to the wall in the backward motion by the simple control. The complex designs of the actuation systems were implemented to improve the magnetic actuation [29]. In addition, the accurate position control of the internal mass with feedback was applied to relatively large robots [18]. As indicated above, self-propelled robots have been actively studied and are very interesting for their dynamics analysis and control. While control aspects are important, it is also significant to realize simple structures and drive methods for the implementation and application of real systems.

This paper proposes a self-propelled board with the slider-crank mechanism for the inclined reciprocal rectilinear motion of the internal mass, which is named KF Board, simplifying Kamamichi-Furuta Board. The distinctive feature of the KF board is that the control input can be set constant in one direction during the locomotion, contrary to that the torque for pendulum of the pendulum-driven cart and the driving force for the internal mass of the capsubot are controlled with switching from forward to backward direction in the one cycle of the reciprocal motion. Our proposed method is advantageous for implementation because of the simplicity of the structure and the driving signal. This driving signal is different from that in [28], which has given the mathematical analysis of the capsubot by the inclined sliding reciprocal motion induced by using the other type of the driving signal, which is not generated by the slider-crank mechanism.

Fig. 3 Friction board with inclined slider presented in [27]

In the following sections, the KF board is firstly presented, and a mathematical model of the system is derived considering a kinematics of the slide-crank mechanism and the constraint conditions of the whole dynamics, where the dynamic friction is only considered in all phases of motion. The effects of inclined angle and the repetitive frequency of the sliding motion of the internal mass are analyzed for the mathematical model. The sliding internal mass connected to the crank shaft works effective compared to the simple swinging pendulum for locomoting the board, since the friction can be made smaller for the cart forward motion by sliding the internal mass downward with acceleration on the inclined guide. If the angle of the inclined guide is steep in downward movement of the internal mass, the pressure for the friction of the cart shall be made smaller in the forward locomotion. Thus, the friction of the cart can be adjusted by the inclined angle. The locomotion speed is shown to be controlled by adjusting the frequency and/or the angle of reciprocal movement of the internal mass. The frequency is controlled by the rotational velocity of the crank shaft. The collision of the internal mass to the stop wall is avoided. The properties of the proposed friction board with the slider-crank mechanism are studied by simulation using the mathematical model derived based on the projection method [30, 31]. From the verifications, the proposed locomotion board with reciprocal motion of the internal motion by using the slider-crank mechanism [32] is shown to move faster when the frequency of the rotation of the crank disk becomes high. The motion of the internal mass is extended to 2D near elliptic orbit by the choice of its position on the connecting rod from the crank to the slider. The simulation is done for the

simplified model with 2D orbital motion of the internal mass. This kind of the locomotive system may be used effectively in the future on the planet where the gravity and friction are small comparing with the earth.

2 Friction board with slider-crank mechanism

In this paper, the friction board with the simple slider-crank mechanism, the KF board, is firstly proposed, where the rectilinear reciprocal motion of the internal mass on a inclined guide is realized by the simple mechanism. Simple control of the fixed given torque can be applied for the rotation of the crank disk.

2.1 Motion mechanism

The KF board consists of the board on the ground and the slider-crank mechanism for generating periodic motion of the internal mass. The slider-crank mechanism is installed with given inclined angle on the board, and can convert the rotational motion into reciprocal motion.

Figure 4 shows the motion principle of the KF board. The KF board is moving by reciprocal motion of the inclined slider. Due to the vertical component of the slider's acceleration, the friction force exerting between the board and ground surface changes as a function of slider's motion. By utilizing this effect, the KF board is possible to locomote by simple reciprocal motion of the slider.

As the crank is rotating at a constant speed, the acceleration of the slider switches between positive and negative according to the rotational angle of the crank. Figure 4a shows downward acceleration of the slider along the inclined guide. Considering the vertical and horizontal decomposition, the slider has downward and leftward acceleration. The board is subjected to the reaction forces generated by this acceleration. The vertical reaction force affects the normal force and then causes a change in the friction force. In this case, the normal force becomes smaller and the friction force also becomes smaller. The horizontal reaction force affects the driving force of the board. The propulsive force of the board increases due to the decrease in friction force. On the other hand, Fig. 4b shows upward acceleration of the slider along the inclined guide. Considering with the same way as above, in this case, the normal force becomes larger and the friction force also becomes larger. The propulsive force of the board decreases due to the increase in friction force.

2.2 Modeling

In this subsection, the mathematical modeling for numerical analysis of the KF board system is presented. Before considering whole dynamics, we focus on the kinematics of the slider-crank mechanism. A schematic diagram of the slider-crank mechanism is shown in Fig. 5. We set the physical parameters as follows; the crank length is r, and the connecting rod length is l. In addition, the angle of the crank is θ and the angle of the connecting rod is ϕ.

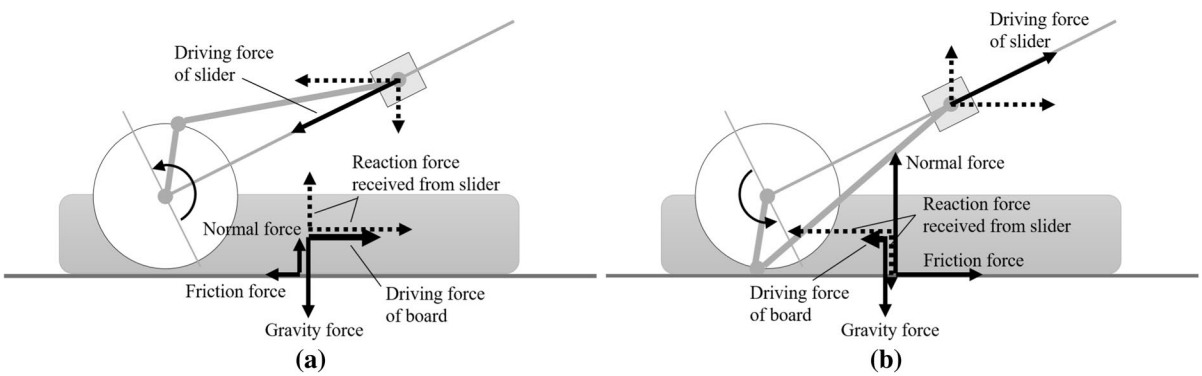

Fig. 4 Motion principle of KF board as the friction force exerting between the board and ground surface changes as a function of slider's motion due to the vertical component of the slider's acceleration. **a** The case of downward acceleration of the slider. **b** The case of upward acceleration of the slider

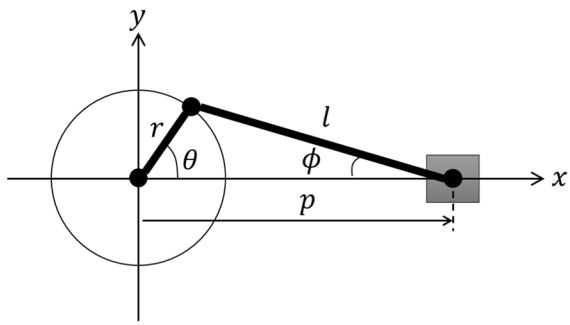

Fig. 5 Model of slider-crank mechanism

The slider is assumed to move along the x axis, and then the position of the slider p is given as

$$p = r\cos\theta + l\cos\phi. \tag{1}$$

The ratio of the crank length to the connecting rod is $\lambda = r/l$. From the relationship of angles, $\cos\phi = \sqrt{1-\sin^2\phi}$ and $\sin\phi = \lambda\sin\theta$, the Eq. (1) can be re-written as

$$p = r\left(\cos\theta + \frac{1}{\lambda}\sqrt{1-\lambda^2\sin^2\theta}\right). \tag{2}$$

Differentiating of the Eq. (2), the velocity relation of the mechanism is derived as

$$\dot{p} = -r\left(\sin\theta + \frac{\lambda\sin 2\theta}{2\sqrt{1-\lambda^2\sin^2\theta}}\right)\dot{\theta}. \tag{3}$$

Note that when r is considerably smaller than l, that is $\lambda \approx 0$, the equations of the slider position and velocity are approximated as

$$p \approx r\cos\theta + l \tag{4}$$

$$\dot{p} \approx -r\sin\theta\dot{\theta}. \tag{5}$$

Then, we consider the motion equation of the board system with the slider-crank mechanism, shown in Fig. 6. The parameters of the system are shown in Table 1.

First, without considering constraints imposed by the slider-crank mechanism, motion equations of the mass M approximating the main body of the board, the slider m and the rotating body (motor) are individually given as

$$\begin{aligned} M\ddot{x}_1 + \mathrm{sgn}(\dot{x}_1)\mu N &= 0 \\ m\ddot{x}_2 &= 0 \\ m\ddot{y}_2 + mg &= 0 \\ I\ddot{\theta} + d_c\dot{\theta} &= u \end{aligned} \tag{6}$$

Table 1 Physical parameters of the KF board system

Notation	Unit	Explanation
x_1	[m]	Board position
x_2, y_2	[m]	Slider position
θ	[rad]	Crank angle
M	[kg]	Board mass
m	[kg]	Slider mass
r	[m]	Crank length (disk radius)
l	[m]	Connecting rod length
I	[kgm^2]	Inertia of disk and motor shaft
d_c	[Nms]	Viscous coefficient of disk and motor shaft
g	[m/s^2]	Gravity acceleration
μ		Friction coefficient
φ	[rad]	Slider angle
u	[Nm]	Input motor torque

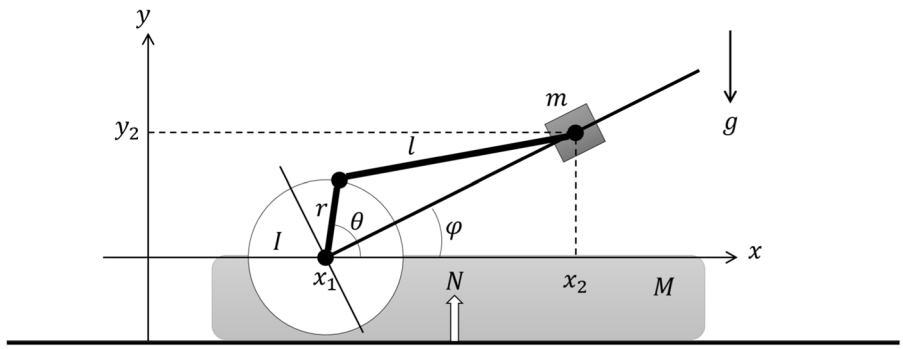

Fig. 6 Model of the KF board system

where μ is a friction coefficient and the normal force on the horizontal surface N is expressed as

$$N = (M+m)g + m\ddot{y}_2. \tag{7}$$

The generalized coordinates are set as $x = [x_1, x_2, y_2, \theta]^T$, and then the Eq. (6) is expressed as

$$D\ddot{x} = h + bu \tag{8}$$

where

$$D = \begin{bmatrix} M & 0 & \mathrm{sgn}(\dot{x}_1)\mu m & 0 \\ 0 & m & 0 & 0 \\ 0 & 0 & m & 0 \\ 0 & 0 & 0 & I \end{bmatrix},$$

$$h = \begin{bmatrix} -\mathrm{sgn}(\dot{x}_1)\mu(M+m)g \\ 0 \\ -mg \\ -d_c\dot{\theta} \end{bmatrix}, \quad b = \begin{bmatrix} 0 \\ 0 \\ 0 \\ 1 \end{bmatrix}.$$

Next, we consider the constraints by the slider-crank mechanism. From the Eq. (2) and the slider's angle φ, the equations of the velocity constraints are given as

$$\begin{cases} \dot{x}_2 - \dot{x}_1 &= -r\cos\varphi X(\theta)\dot{\theta} \\ \dot{y}_2 &= -r\sin\varphi X(\theta)\dot{\theta} \end{cases} \tag{9}$$

where $X(\theta) = \sin\theta + \frac{\lambda\sin 2\theta}{2\sqrt{1-\lambda^2\sin^2\theta}}$. The Eq. (9) is expressed in matrix form as

$$J\dot{x} = 0 \tag{10}$$

where the Jacobian J is given as

$$J = \begin{bmatrix} -1 & 1 & 0 & r\cos\varphi X(\theta) \\ 0 & 0 & 1 & r\sin\varphi X(\theta) \end{bmatrix}. \tag{11}$$

Differentiating of the constraint Eq. (10),

$$J\ddot{x} + \dot{J}\dot{x} = 0 \tag{12}$$

is given.

Finally, the motion equation considering with constraint is given as

$$D\ddot{x} = h + bu - J^T\lambda_f \tag{13}$$

where λ_f is a constraint force. From the Eqs. (12) and (13),

$$\begin{bmatrix} D & J^T \\ J & 0 \end{bmatrix}\begin{bmatrix} \ddot{x} \\ \lambda_f \end{bmatrix} = \begin{bmatrix} h + bu \\ -\dot{J}\dot{x} \end{bmatrix} \tag{14}$$

is given. The motion of the simple friction board system can be analyzed by using above equation.

Here, independent generalized coordinates can be defined as $q = [x_1, \theta]^T$.The relation between x and q is represented as

$$\dot{x} = Q(q)\dot{q} \tag{15}$$

where

$$Q(q) = \begin{bmatrix} 1 & 0 \\ 1 & -r\cos\varphi X(\theta) \\ 0 & -r\sin\varphi X(\theta) \\ 0 & 1 \end{bmatrix}. \tag{16}$$

The matrix Q is the orthogonal complement matrix to J, satisfying the relation of $JQ = 0$. Multiplying the Eq. (13) by Q^T from the left-hand side and substituting the Eq. (15), the constraint force can be vanished and the motion equation with generalized coordinates is represented as

$$Q^TDQ\ddot{q} = Q^T(-D\dot{Q}\dot{q} + h + bu). \tag{17}$$

Calculating the Eq. (17), the explicit form of the motion equation can be derived as

$$\begin{bmatrix} M+m & -mr\cos\varphi X(\theta) - \mu mr\mathrm{sgn}(\dot{x}_1)\sin\varphi X(\theta) \\ -mr\cos\varphi X(\theta) & mr^2X^2(\theta) + I \end{bmatrix}\begin{bmatrix} \ddot{x}_1 \\ \ddot{\theta} \end{bmatrix} = \begin{bmatrix} mr\cos\varphi\dot{X}(\theta)\dot{\theta} + \mu\mathrm{sgn}(\dot{x}_1)\{mr\sin\varphi\dot{X}(\theta)\dot{\theta} - (M+m)g\} \\ -mr^2X(\theta)\dot{X}(\theta)\dot{\theta} - mrg\sin\varphi X(\theta) - d_c\dot{\theta} + u \end{bmatrix}. \tag{18}$$

Note that the inertia matrix of motion Eq. (18) is asymmetric, as the asymmetric term is caused by the friction force changes in response to the vertical acceleration of the slider mass. In addition, in case that the crank length r is smaller than the connecting rod length l, that is $\lambda \approx 0$, approximations of the kinematical relation can be obtained as $X(\theta) \approx \sin\theta$ and $\dot{X}(\theta) \approx \cos\theta\dot{\theta}$. From the equations, the motion equation can be approximated as

$$\begin{bmatrix} M+m & -mr\cos\varphi\sin\theta - \mu mr\mathrm{sgn}(\dot{x}_1)\sin\varphi\sin\theta \\ -mr\cos\varphi\sin\theta & mr^2\sin^2\theta + I \end{bmatrix}\begin{bmatrix} \ddot{x}_1 \\ \ddot{\theta} \end{bmatrix} = \begin{bmatrix} mr\cos\varphi\cos\theta\dot{\theta}^2 + \mu\mathrm{sgn}(\dot{x}_1)\{mr\sin\varphi\cos\theta\dot{\theta}^2 - (M+m)g\} \\ -mr^2\sin\theta\cos\theta\dot{\theta}^2 - mrg\sin\varphi\sin\theta - d_c\dot{\theta} + u \end{bmatrix}. \tag{19}$$

3 Motion analysis

To investigate the motion of the KF board system, numerical simulations are done using MATX, and experiments are demonstrated using a simple apparatus assembled by LEGO components. In addition, simplified model simulations with 2D orbital motion of the internal mass are investigated as extensions of the slider-crank mechanism.

3.1 Numerical simulations

The motion of the KF board system is analyzed using non-approximate dynamical model derived in the previous section. Physical parameters in Table 1 are set as $M = 0.2$ kg, $m = 0.2$ kg, $r = 0.025$ m, $l = 0.085$ m, $I = 2.0\times10^{-5}$ kgm^2, $d_c = 0.01$ Nms, $g = 9.81$ m/s^2. The friction coefficient is set to $\mu = 0.3$ as moderate slipping condition. The angle of the slider is set as $\varphi = \pi/6$ rad.

Figures 7 and 8 show the results of numerical simulation, where constant input torque is applied to the motor. The crank rotates in one direction by the constant input torque. Its rotating velocity is approximately constant, with a few fluctuations due to the gravity force acting to the slider. Corresponding to the rotation of the crank motion, the slider is reciprocating along the inclined angle. The reciprocal motion of the slider makes the board move forward with repeating forward and slight backward movements.

The simulations show that the rotating velocity of the crank and the frequency of the gait are proportional to the input torque. In the case of Fig. 8, the rotating velocity and the frequency of the gait are higher comparing to Fig. 7, since the input torque is large. In case that the forward velocity of the board is fast, the backward velocity is correspondingly fast. The backward moving distance is quite small compared to the forward moving distance. As the results, the moving distance per one cycle and the average velocity become large.

Figure 9 shows the closeup of one cycle motion of the friction board in Fig. 7. Figure 9a shows the time history of mass positions and the relative position between the board and the slider mass, and Fig. 9b shows the phase plane. The section of each motion step is indicated on the figure. From this figure, the transition of the motion step is observed. The motion of the internal mass and the board follows mostly Step 1, 2, and Step 4' instead of Step 4, where Step 4': Forward slow motion of the internal mass causes the slow backward movement of the main body. During this motion the main body slowly moves backward, where the distance loss can be designed to be small.

To verify the motion characteristics, numerical simulations under different input torques are conducted. The verification results are shown in Fig. 10. Figure 10a shows the moving distance per one cycle of the board, and Fig. 10b shows its average velocity. As described above, the frequency of the gait is proportional to the input torque. As shown in Fig. 10a, the moving distance per one cycle increases linearly with increasing the frequency of the gait up to a certain frequency, and decreases slightly in higher frequency. As the frequency of the gait becomes higher, the acceleration of the reciprocal motion becomes large. Thus, the moving distance for one cycle becomes large in a certain lower region of frequencies, however; the moving distance in higher gait frequency decreases due to the increase of backward distance. When the gait frequency increases, the forward motion in Step 1 and 2 becomes larger, however; the backward motion in Step 4' becomes also larger. As the results, the moving distance per one cycle decreases in high gait frequency. As shown in Fig. 10b, the average velocity of the board increases with increasing the gait frequency.

In addition, to verify the effect of the inclined angle of the slider, numerical simulations under difference angles are conducted. The verification results are shown in Fig. 11. The average velocities of the board with respect to inclined angles of the slider are analyzed for three different input torques. The average velocities change significantly depending on the inclined angle. Due to the nonlinear characteristics of the slider-crank mechanism, the average velocities are slightly shifted in the positive direction. As the input increases, the gait frequency increases, and correspondingly the average velocity increases. The inclined angle to maximize the velocity tends to larger as the gait frequency increases, in the range of the simulation conditions.

3.2 Assembling KF board and experiment

The KF board system can be implemented simply by use of the slider-crank mechanism. In this paper, the

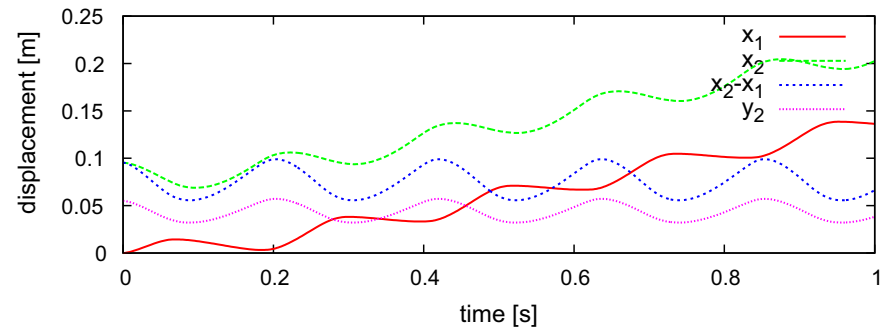

(a)

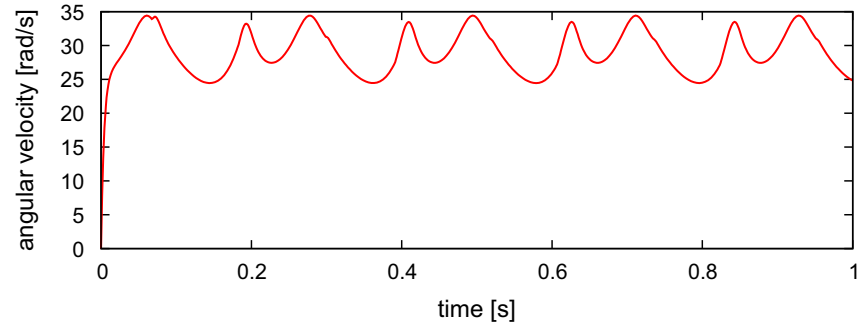

(b)

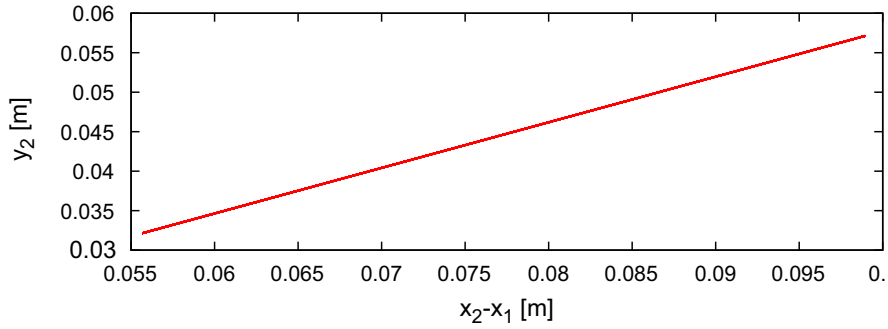

(c)

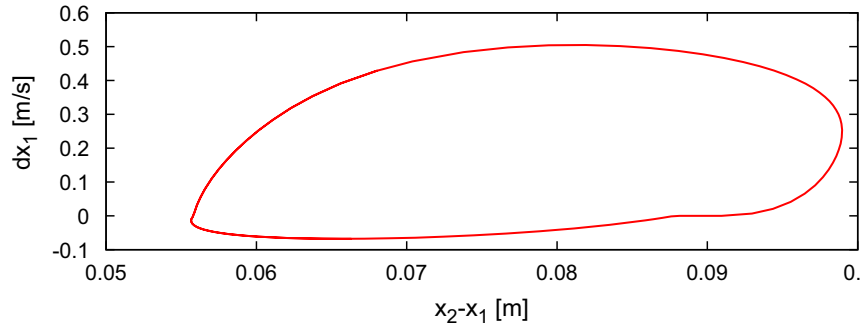

(d)

Fig. 7 Simulation result of the friction board motion with input torque $u = 0.3$: **a** horizontal positions of the board and the slider x_1, x_2, relative position between x_1 and x_2, and vertical position of the slider y_2, **b** angular velocity of the crank $\dot{\theta}$, **c** relative trajectory of the slider with respect to the board, **d** phase plane of the motion plotting velocity variation of the board $\dot{x}_1$ as a function of relative position between x_1 and x_2

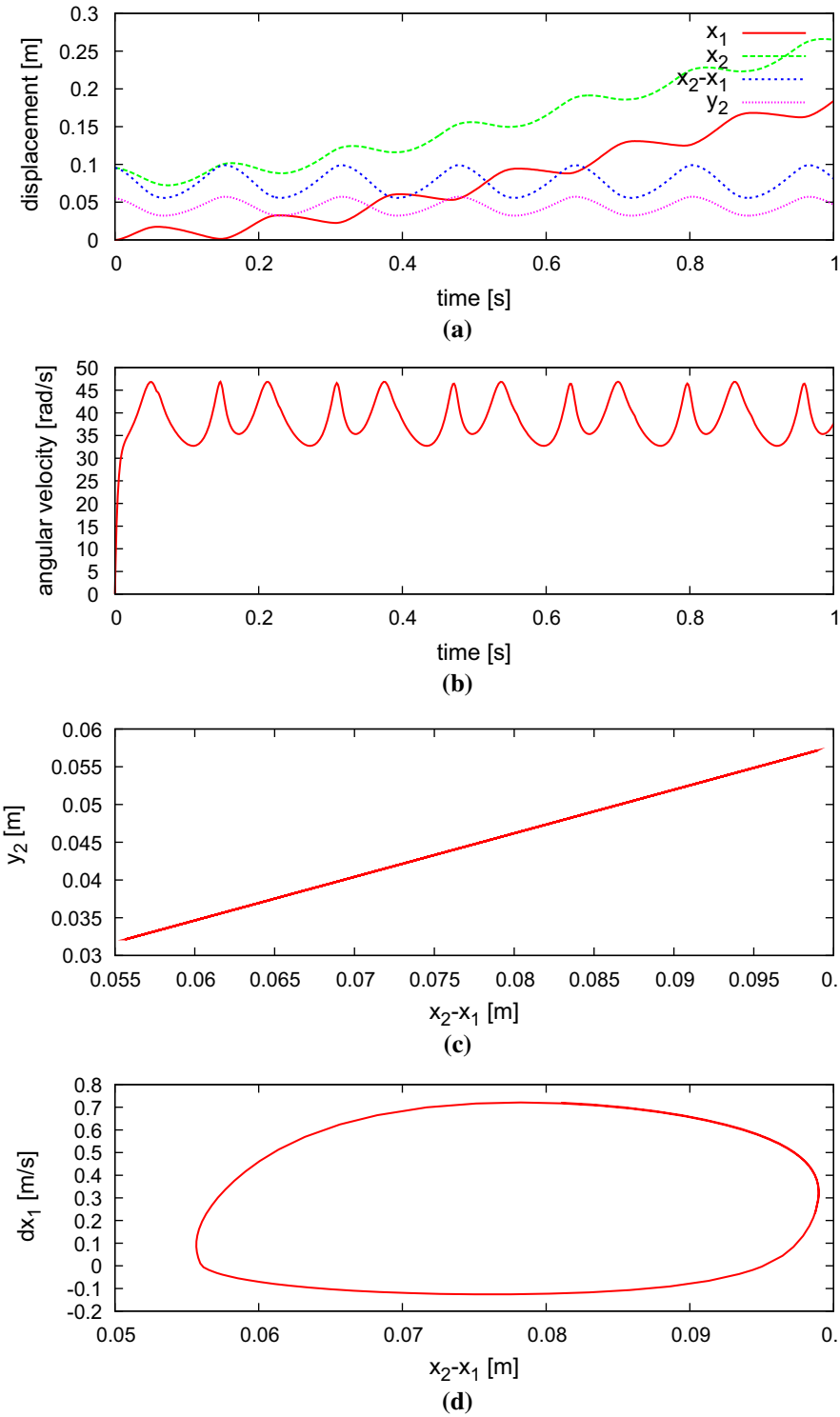

Fig. 8 Simulation result of the friction board motion with input torque $u = 0.4$: **a** horizontal positions of the board and the slider x_1, x_2, relative position between x_1 and x_2, and vertical position of the slider y_2, **b** angular velocity of the crank $\dot{\theta}$, **c** relative trajectory of the slider with respect to the board, **d** phase plane of the motion plotting velocity variation of the board $\dot{x}_1$ as a function of relative position between x_1 and x_2

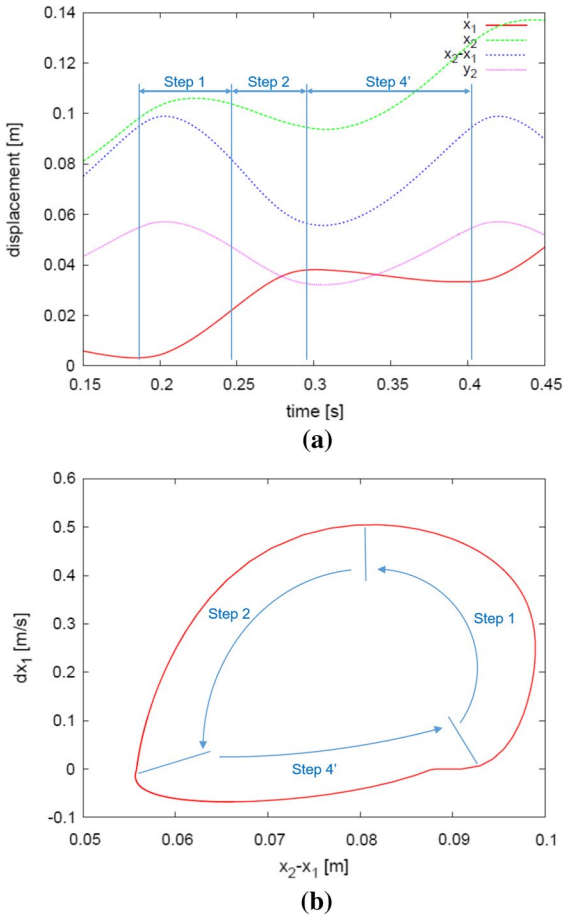

Fig. 9 Motion analysis of the friction board in one period with closeup of Fig. 7: **a** time history of the motion, **b** phase plane

KF board is assembled by using LEGO Mindstorms EV3 blocks, as shown in Fig. 12. A crank disk is attached on a motor shaft and connected to a connecting rod. The connecting rod is connected to the sliding internal mass placed on an inclined linear guide. Due to the small power of the motor, the driving force of the board is limited. To reduce the friction between the board and the floor, tire wheels are installed.

The motor drives the crank, and the sliding mass reciprocates linearly on the guide. When the crank rotates one revolution, the sliding mass reciprocates one time with a stroke of twice the crank length, where the direction of the rotation is taken arbitrary, and in this paper, the anticlockwise direction is taken regularly.

Figure 13 shows serial photographs of the experimental test of the KF board, which are captured from a video image at interval of 0.1 s. Figure 15 shows the experimental data of the KF board motion, measured by using a motion capture system (OptiTrack V120: Trio), and the simulation results are also plotted for comparison. From the results, it can be observed that the KF board moved rightward as the slider-crank mechanism reciprocates. When the slider moves toward lower left side, the board moves rightward. When the slider moves toward upper right side, the board moved back slightly. As a result of repeating motions of the slider-crank mechanism, the board can locomote.

The experimental results are compared to those computed by simulation. The parameters of the simulation model are identified from preliminary experiments. First, the equivalent mass for the tireless board model is identified. As shown in Fig. 14, the board is connected to a weight with a string, and the string is hung on a pulley. By the gravity force of the weight, the board moves in uniformly accelerated motions. Then the accelerations for two different weights are determined from the trajectory of movements. The motion equations of the experiment are represented as

$$\begin{aligned}(M_c + W_1)a_1 &= W_1 g - F \\ (M_c + W_2)a_2 &= W_2 g - F\end{aligned} \tag{20}$$

where M_c is the equivalent mass of the board ($M_c = M + m$), W_1, W_2 are the weights of the masses, a_1, a_2 are corresponding accelerations, g is the gravity acceleration, and F is the friction force. Subtracting the lower from the upper Eq. (20), the equivalent mass is derived as

$$M_c = \frac{W_1(g - a_1) - W_2(g - a_2)}{a_1 - a_2}. \tag{21}$$

Next, the input torque u is determined to match the motion frequency of the experiment. Finally, the friction coefficient μ is determined to match the displacement of the experiment.

From the above procedures, the simulation parameters are set as $M = 0.111$ kg, $m = 0.059$ kg, $u = 0.182$ Nm, $\mu = 0.08$. The angle of the slider is $\pi/9$, and the other parameters are set as the same conditions of the previous subsection. From Fig. 15, it can be confirmed that the experiment and the simulation agree well including forward and slight backward behavior.

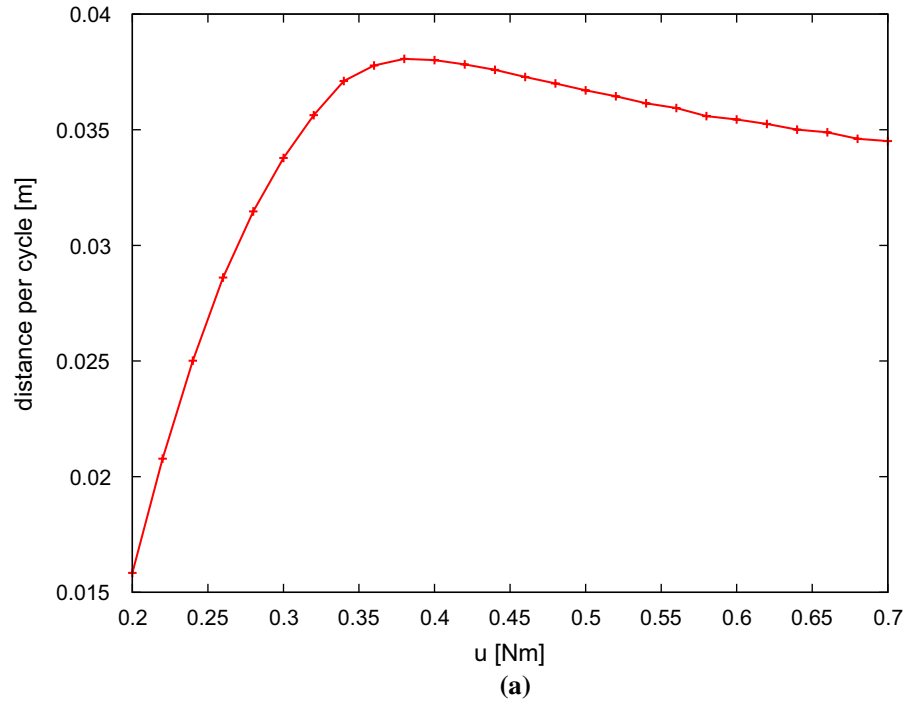

(a)

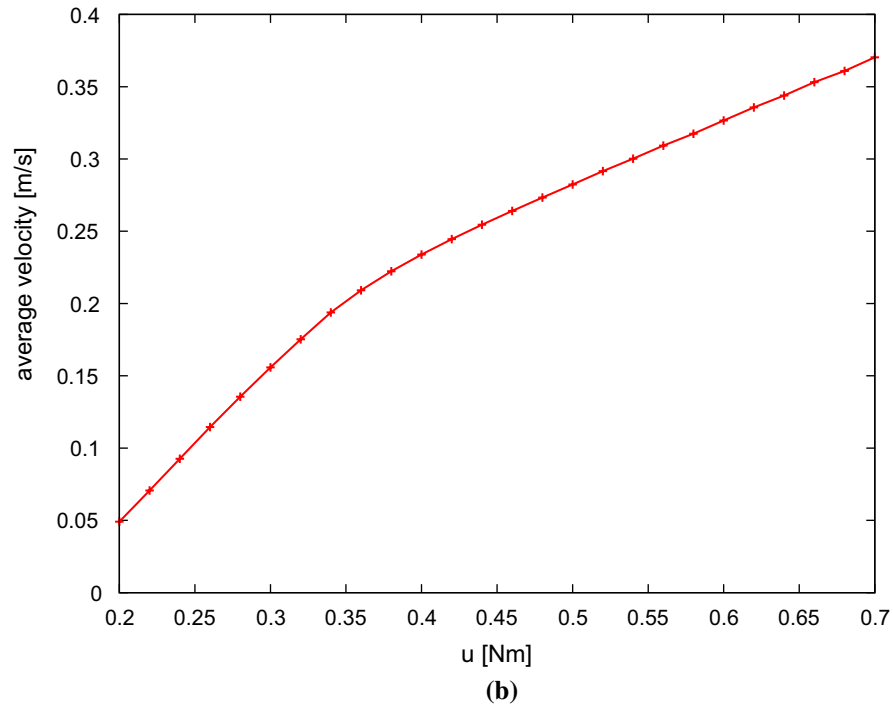

(b)

Fig. 10 Motion analysis of the friction board with input changes: **a** displacement per cycle and **b** average velocity as a function of input torque u

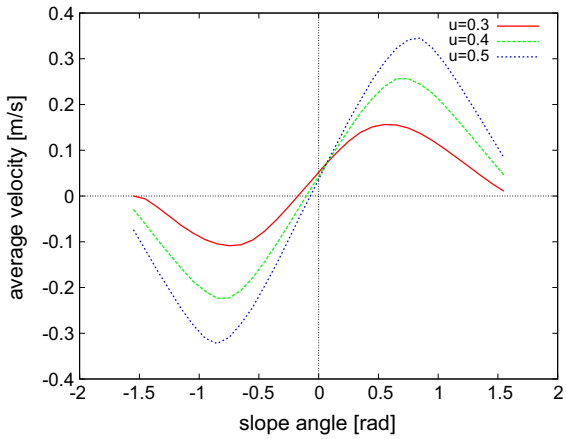

Fig. 11 Motion analysis of the friction board with slider's angle changes: average velocities as a function of inclined angle φ for input torques $u = 0.3, 0.4, 0.5$

3.3 Simplified model simulations with 2D orbital motion of the internal mass

In this subsection, motion analysis using simplified model with 2DOF internal mass motion, which has horizontal and vertical movements of an internal mass, is theoretically investigated. This model can capture the approximated dynamics of the friction board with slider-crank mechanism, as the appropriate input signals are selected. In addition, extended motions can be considered for realizing more efficient locomotion. In the friction board with slider-crank mechanism presented in the previous section, the motion of the sliding internal mass is constrained to 1 DOF surface. If the freedom of the motion of the internal mass is augmented to 2DOF, the locomotion performance is expected to be improved.

Figure 16 shows images of the extended motion of the internal mass. When the slider mass is larger than the moving link, the motion of the moving internal mass is considered to be linear reciprocal motion. On the contrary, the connecting rod mass as the moving link is larger than the slider mass, the motion of internal mass is considered to be near-elliptical. Especially, as the crank length r is considerable smaller than the connecting rod length l, that is $\lambda \approx 0$, the trajectory of the moving mass can be approximated to complete ellipse.

The KF board with 2D orbital motion can be modelled similar to Sect. 2.2. As a simple extension model, the moving mass is assumed to be located on the connecting rod as shown in Fig. 17. The slider is hereby also assumed to move along the x axis, and then the position of the moving mass (p_x, p_y) is given as

$$\begin{cases} p_x = r\cos\theta + kl\cos\phi = r\left(\cos\theta + \frac{k}{\lambda}\sqrt{1-\lambda^2\sin^2\theta}\right), \\ p_y = l(1-k)\sin\phi = r(1-k)\sin\theta, \end{cases} \tag{22}$$

where k is the ratio of the distance of the moving mass from the joint to whole length of the connecting

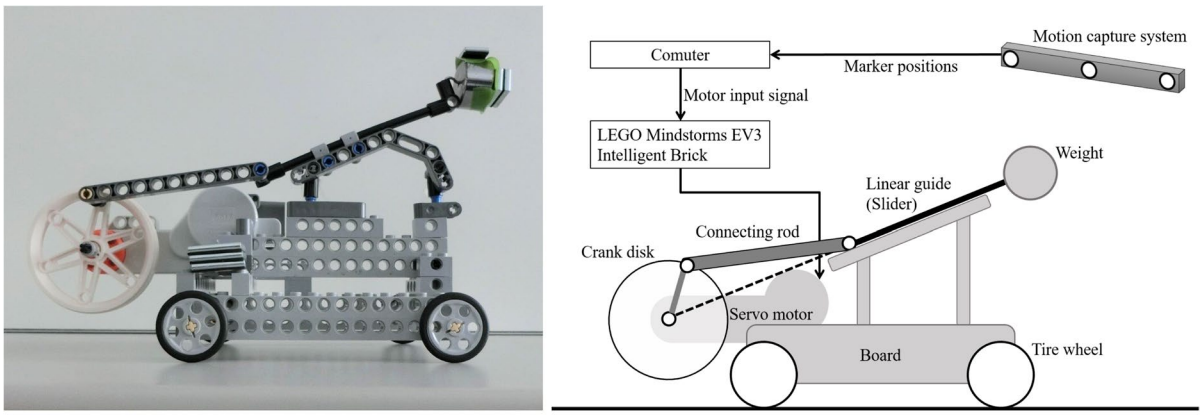

Fig. 12 Experimental setup of KF Board: **a** photograph of the KF board assembled by using LEGO Mindstorms, **b** schematics of the experimental system

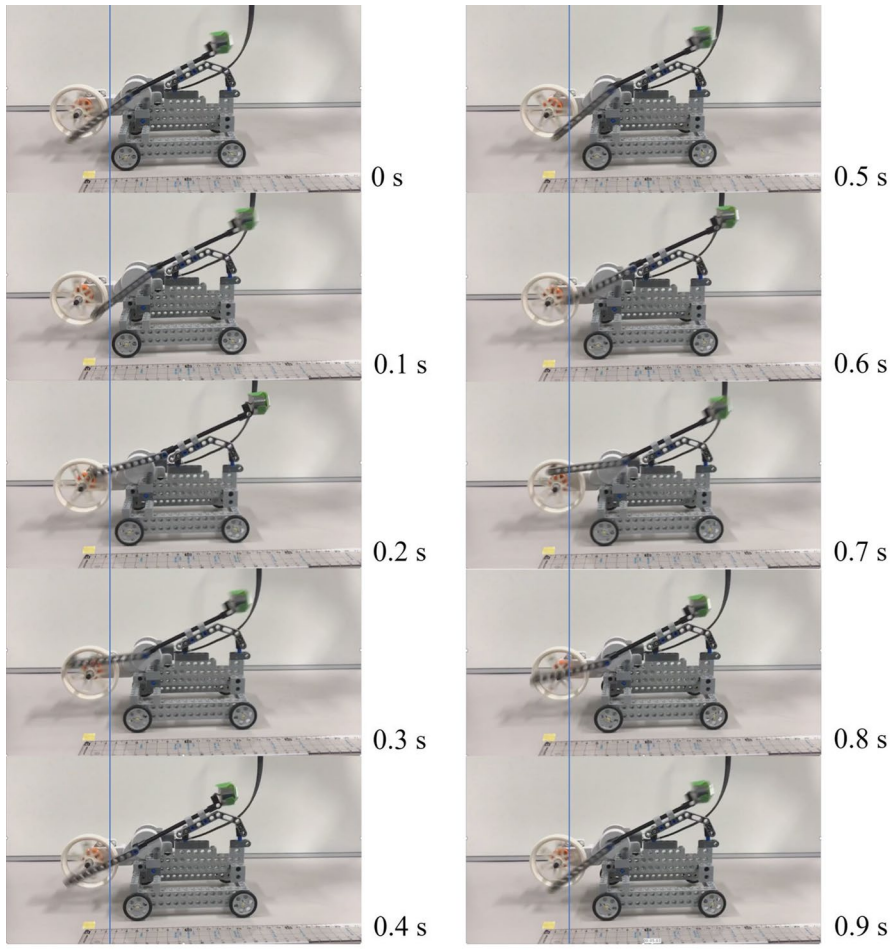

Fig. 13 Experimental setup for identificating the equivalent mass

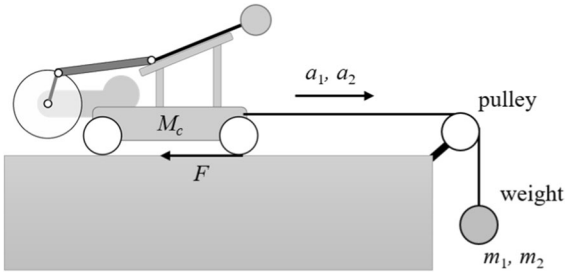

Fig. 14 Serial photographs of experimental test of the KF board

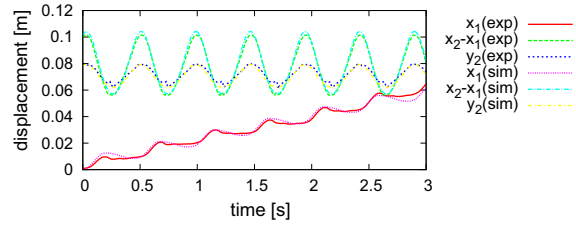

Fig. 15 Experimental and simulation results of the KF board motion: horizontal positions of the board, relative position between x_1 and x_2, and vertical position of the slider y_2

rod, that is, the distance of the moving mass is kl. If r is considerably smaller than kl and $\lambda \approx 0$, p_x of the Eq. (22) is approximated as

$$p_x \approx r\cos\theta + kl. \tag{23}$$

As described above, it is confirmed that the approximated trajectory of the moving mass becomes complete ellipse. In Fig. 17, k is chosen as $0 < k < 1$, and the other cases are also interesting.

Differentiating of the Eq. (22), the velocity relations of the mechanism are derived as

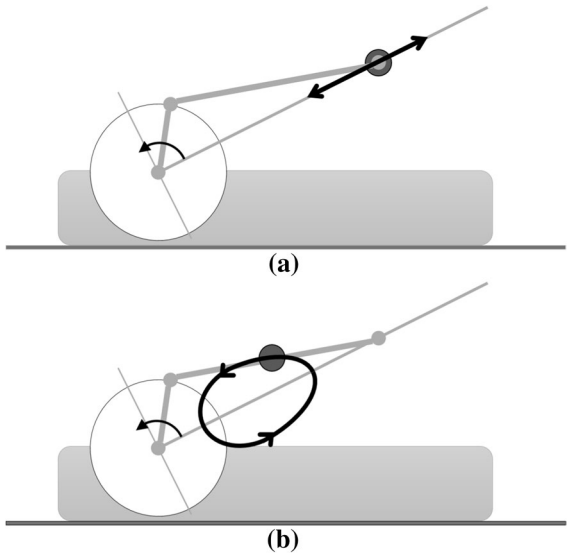

Fig. 16 Images of the extended internal motions: **a** linear motion on the slider, **b** periodic two-dimensional plane motion

$$\begin{cases} \dot{p}_x = -r\left(\sin\theta + \frac{k\lambda\sin 2\theta}{2\sqrt{1-\lambda^2\sin^2\theta}}\right)\dot{\theta}, \\ \dot{p}_y = r(1-k)\cos\theta\dot{\theta}. \end{cases} \tag{24}$$

Considering the constraints by the slider-crank mechanism in the KF board, the equations of the velocity constraints are given from the Eq. (24) and the slider's angle φ, as

$$\begin{bmatrix} \dot{x}_2 - \dot{x}_1 \\ \dot{y}_2 \end{bmatrix} = \begin{bmatrix} \cos\varphi & -\sin\varphi \\ \sin\varphi & \cos\varphi \end{bmatrix} \begin{bmatrix} \dot{p}_x \\ \dot{p}_y \end{bmatrix}. \tag{25}$$

Simple periodic patterns not only linear motion but also curved two-dimensional orbital motion can be realized by simple mechanisms such as a link

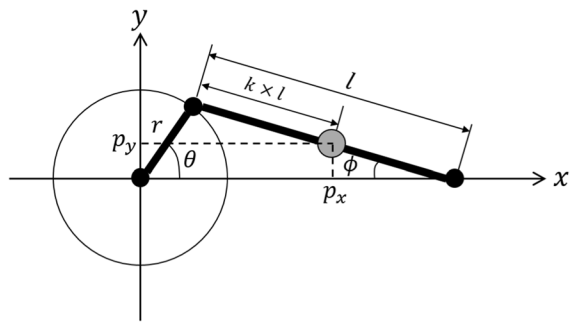

Fig. 17 Extended Model of slider-crank mechanism

mechanics or a cam mechanics. Therefore, in this subsection, motion analysis using simplified model, which can express the augmented 2DOF internal mass motions, is investigated.

Figure 18 shows analytic model of the simplified model with 2DOF inputs. The model is expressed as a two mass system, an outer frame and an internal mass. The x coordinate of the center of gravity position of the outer frame is x_1, and the center of gravity position of the internal mass is $(x_2\ ,\ y_2)$. The mass of the outer frame is m_1 and the internal mass is m_2. The input forces are acting between the outer frame and the internal mass. The force of the horizontal direction is u_1 and one of the vertical direction is u_2. The friction between the outer frame and the internal mass is assumed to be negligible. The friction coefficient between the outer frame and the ground is μ. The gravity acceleration is g. From Fig. 18, the motion equation of the simplified model with 2DOF inputs is given as

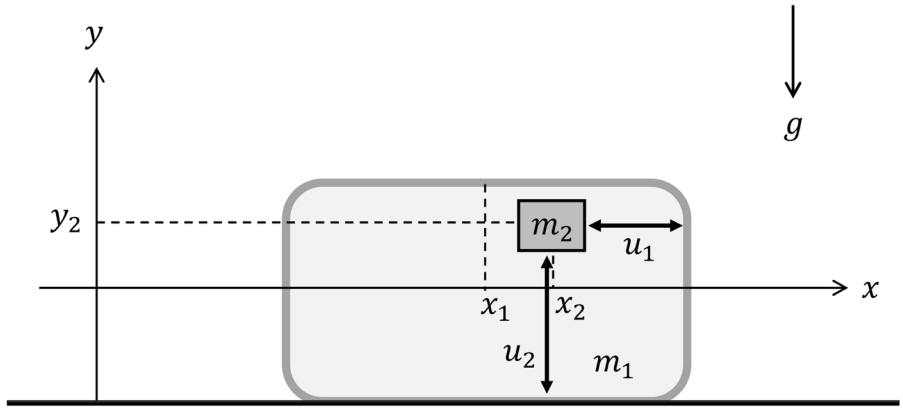

Fig. 18 Model of simplified analysis model with 2DOF internal mass motion

$$m_1\ddot{x}_1 + \mathrm{sgn}(\dot{x}_1)\mu(m_1 g - u_2) = u_1 \tag{26}$$

$$m_2\ddot{x}_2 = -u_2 \tag{27}$$

$$m_2\ddot{y}_2 + m_2 g = -u_2. \tag{28}$$

Here, we consider a simple periodic pattern generated by sinusoidal signal. The movements of two directions are controlled by simple harmonic motions with same angular frequency to synchronize both horizontal and vertical movements.

The movement patterns are set as

$$x_2 - x_1 = \alpha\cos(\omega t) \tag{29}$$

$$y_2 = \beta\cos(\omega t + p) \tag{30}$$

where ω is an angular frequency of the input signal, p is a phase difference between the vertical and horizontal movements, and the amplitudes of each direction are α and β.

By applying the given motion of the Eqs. (29) and (30), the internal mass moves along an inclined elliptical orbit in the outer frame. The inclined angle of the elliptical axis is $\tan^{-1}(\beta/\alpha)$. The patterns include a linear motion, as the phase difference p is set to zero. In such pattern, it can be considered to be an approximated pattern of the slider-crank mechanism shown in the Eqs. (4) and (5).

Consider control inputs to realize the motion patterns of the Eqs. (29) and (30). First, the input u_2 for the vertical motion is determined to satisfy the Eq. (30). From the second derivative of Eq. (30) and the Eq. (28), the input u_2 is derived as derived as

$$u_2 = -m_2 g + \beta\omega^2 m_2\cos(\omega t + p) \tag{31}$$

Next, the input u_1 for the horizontal motion is determined to satisfy the Eqs. (29) and (30). From the Eqs. (26) and (27),

$$m_1 m_2(\ddot{x}_2 - \ddot{x}_1) - \mathrm{sgn}(\dot{x}_1)\mu m_2(m_1 g - u_2) = -(m_1 + m_2)u_1 \tag{32}$$

is given. Substituting the second derivative of the Eq. (29) and the Eq. (31), the control input u_1 is derived as

$$u_1 = \frac{m_2}{m_1 + m_2}\left[\alpha\omega^2 m_1\cos(\omega t) + \mathrm{sgn}(\dot{x}_1)\mu\{(m_1 + m_2)g - \beta\omega^2 m_2\cos(\omega t + p)\}\right]. \tag{33}$$

Note that it is necessary to set the parameter so as to keep the outer frame contacting to the ground surface, that is, the normal force to the outer frame should satisfy the following condition:

$$N = (m_1 + m_2)g - \beta\omega^2 m_2\cos(\omega t + p) > 0. \tag{34}$$

To analyze the motion, numerical simulations are conducted using MATX. Parameters of the system are set as m_1 =0.2 kg, m_2 = 0.2 kg, g = 9.81 m/s^2, μ=0.3, $\alpha = 0.025\cos(\pi/6)$ m, $\beta = 0.025\sin(\pi/6)$ m, ω = 30 rad/s, which are set as the same conditions of the simulations in the previous section.

Figure 19 shows the simulation results where the phase difference is $p = 0$ rad. Figure 19a shows the positions of the outer frame x_1, the internal mass x_2, y_2, and their distance in horizontal plane $x_2 - x_1$. Figure 19b shows the input forces u_1, u_2 and the normal force to the outer frame N. Figure 19c shows the trajectory of the internal mass relative to the outer frame. Figure 19d shows the velocity changes of the outer frame $\dot{x}_1$ as a function of relative position between x_1 and x_2.

From Fig. 19a, the forward motion is observed consisting of the repeating forward and slight backward motions. From Fig. 19b, it can be seen that the normal force decreases when the input u_2 increases, and the normal force increases when u_2 decreases, and the normal force increases when u_2 decreases. Therefore, the friction force varies in response to the vertical movement of the internal mass, and their variations of the friction affect the motion.

To investigate the effect of the phase difference of the input signals, numerical analysis with various conditions is performed. The phase difference p varies in the range of $-\pi \le p \le \pi$, and the average velocities are compared. Figure 20 shows the simulation results of the moving distance per one cycle with respect to the phase difference of input signals. From the results, it is confirmed that $p = -0.6$ rad is the fastest condition.

Figure 21 shows the simulation results where the phase difference is $p = -0.6$ rad, as the pattern of the fastest movement. In comparison with the results of Figs. 19 and 21, the pattern of $p = -0.6$ gives

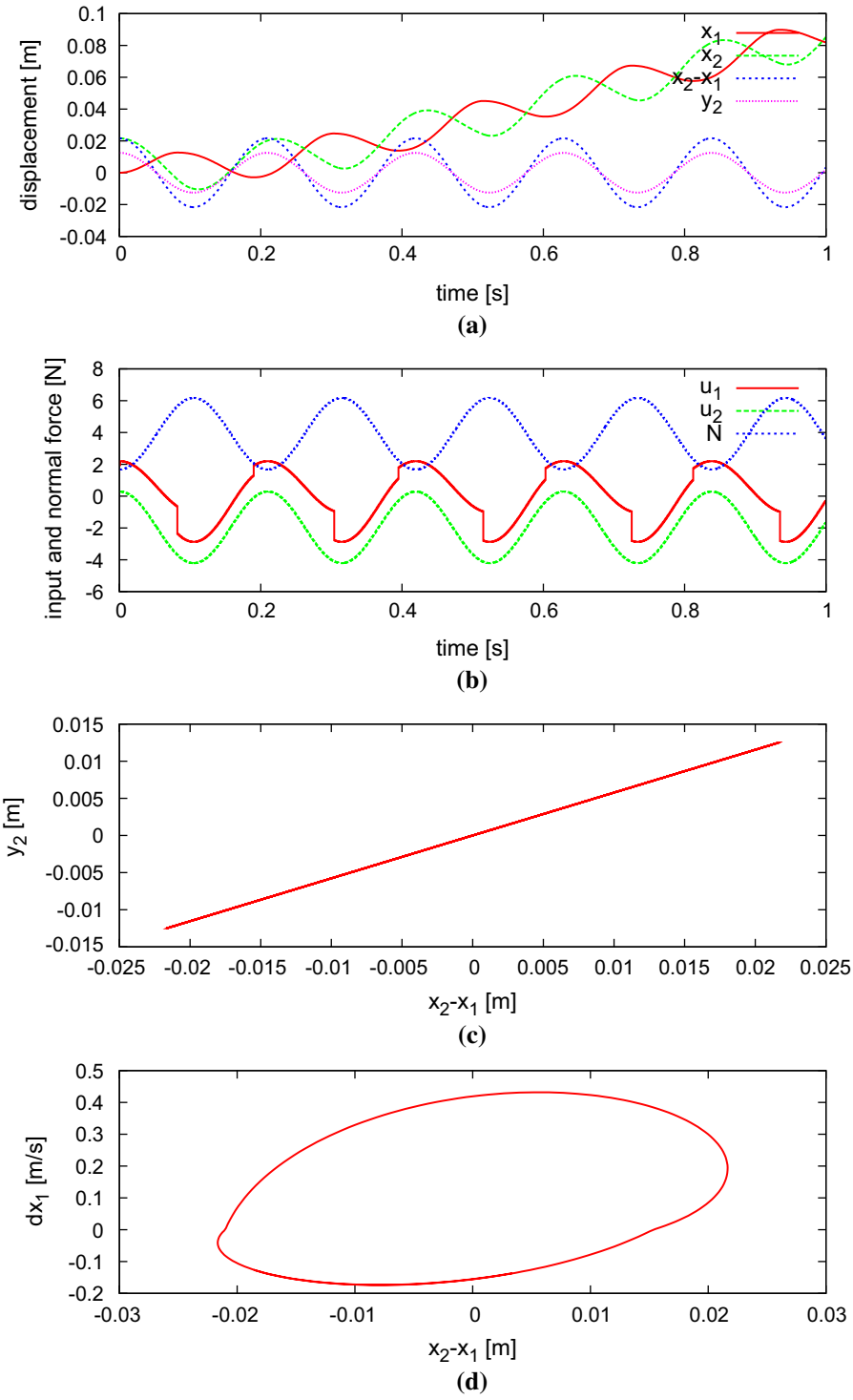

Fig. 19 Simulation result of the simplified model with phase difference of inputs $p = 0$ rad: **a** horizontal positions of the outer frame and the internal mass x_1, x_2, relative position between x_1 and x_2, and vertical position of the internal mass y_2, **b** input forces of horizontal and vertical directions u_1, u_2 and normal force to the outer frame N, **c** relative trajectory of the internal mass with respect to the outer frame, **d** phase plane of the motion plotting velocity variation of the outer frame $\dot{x}_1$ as a function of relative position between x_1 and x_2

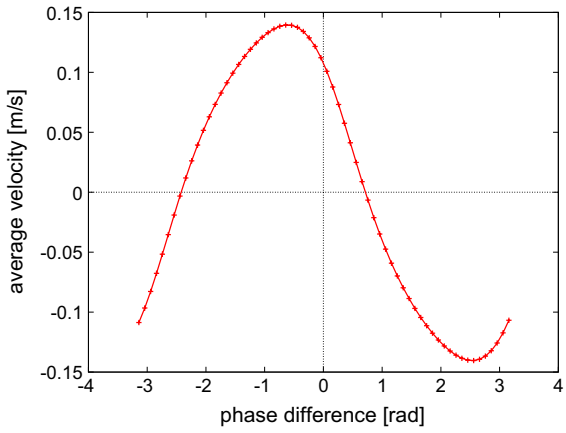

Fig. 20 The average velocity of the simplified model with respect to the phase difference of inputs

obviously faster movement than that of $p = 0$. The locomotive behaviors in one cycle are almost same as the board moves forward with repeating forward and slight backward movements. However, the backward displacement in $p = -0.6$ is smaller than $p = 0$. This is caused by the interaction of the normal force acceleration of internal mass. As the results, the phase difference of the input signals affects to the locomoting motion.

4 Conclusion

This paper proposes the KF board, which is easily realized in the laboratory by using LEGO components. The locomotion of the FK board is done by inputting the constant torque to rotate the crank. The velocity of the locomotion is easily designed from the frequency of the reciprocal motion of the internal mass. The locomotion properties of the KF board have been analyzed by simulation using the mathematical model. The effects of the frequency and the angle of the sliding reciprocal motions to the locomotion are shown as follows: Increasing the frequency of the reciprocal motion of the internal mass is found to bring faster motion of the board up to a certain frequency. Over that frequency, the board moves slower for the higher frequency. Similarly increasing the angle of the slider for reciprocal motion of the internal mass brings the faster motion up to a certain angle, and over the angle, the movement of the board becomes slower. Based on these facts, the appropriate input torque can be determined. Thus, the control design of the KF board is simple and it may be used in many situations like small gravity planet surface. It is remarked that the further study should be done for the systematic design method of the general KF board with 2D orbital motion of the internal mass.

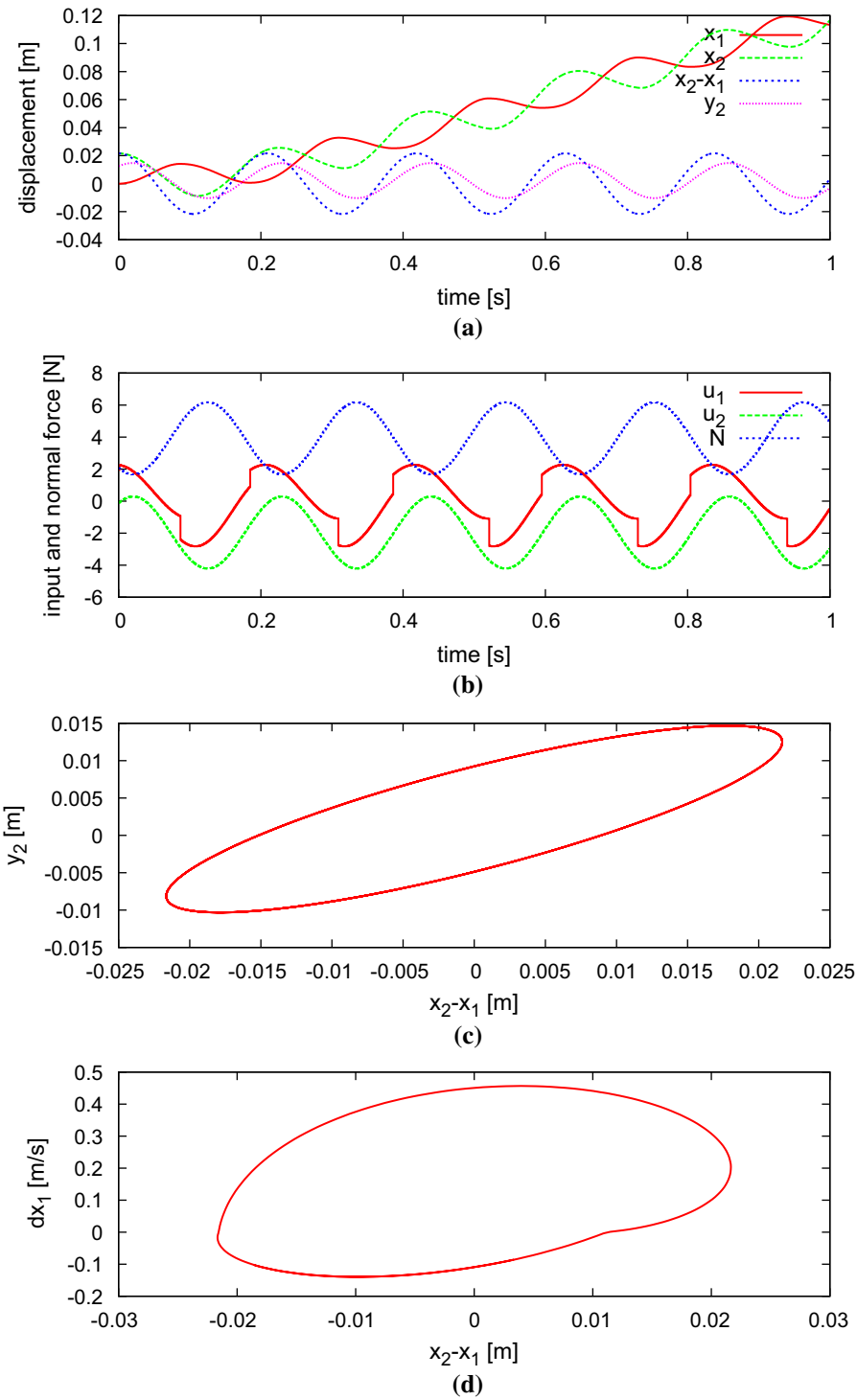

Fig. 21 Simulation result of the simplified model with phase difference of inputs $p = -0.6$ rad: **a** horizontal positions of the outer frame and the internal mass x_1, x_2, relative position between x_1 and x_2, and vertical position of the internal mass y_2, **b** input forces of horizontal and vertical directions u_1, u_2 and normal force to the outer frame N, **c** relative trajectory of the internal mass with respect to the outer frame, **d** phase plane of the motion plotting velocity variation of the outer frame $\dot{x}_1$ as a function of relative position between x_1 and x_2

Acknowledgements The special thanks to Dr. Hongyi Li, General Robots Inc., and Mr. Yoshihiro Suzuki, Canon Co., whose works at Tokyo Denki University have been quite important for writing the paper. The authors thank the reviewer comments for improving the paper and Mr. Shunsuke Sasaki for helping the assembling KF board and achieving the experiments.

Funding This study was funded by the Grant in Aid for COE Research Project and MEXT KAKENHI B Grant Number 24360166.

Declarations

Conflict of interest Conflict of Interest: The authors declare that they have no conflict of interest.

References

1. Chernousko FL (2001) Controllable motion of a two-link mechanism along a horizontal plane. J Appl Math Mech 65:578–591
2. Chernousko FL (2002) The optimum rectilinear motion of a two-mass system. J Appl Math Mech 66:1–7
3. Higuchi T, Yamagata Y, Furutani K, Kudoh K (1990) Precise positioning mechanism utilizing rapid deformation of piezoelectric elements. In: Proc. of IEEE workshop on micro electro mechanical systems, pp 47–49
4. Darby AP, Pellegrino S (1997) Inertial stick-slip actuator for active control of shape and vibration. J Intell Mater Struct 8:1001–1011
5. Mori S, Nishihara H, Furuta K (1976) Control of unstable mechanical systems: control of pendulum. Int J Control 23:673–692
6. Åström KJ, Furuta K (2000) Swinging up a pendulum by energy control. Automatica 36(2):287–295. https://doi.org/10.1016/S0005-1098(99)00140-5
7. Li H, Furuta K, Chernousko FL (2005) A pendulum-driven cart via internal force and static friction. In: Proc. of conf. physics and control, St. Petersburg, Russia, pp 15–17
8. Li H, Furuta K, Chernousko FL (2006) Motion generation of capsubot using internal force and static friction. In: Proc. of IEEE conf. decision and control, San Diego, USA, pp 6575–6580
9. Chernousko FL (2018) Locomotion of multibody robotic systems: dynamics and optimization. Ther Appl Mech 24(1):17–23
10. Liu Y, Yu H, Burrows B (2007) Optimization and control of a pendulum-driven cart-pole system. In: Proc. of IEEE conf. networking, sensing and control, London, UK, pp 152–256. https://doi.org/10.1109/ICNSC.2007.372768
11. Liu Y, Yu H, Cang S (2012) Modelling and motion control of a double-pendulum driven cart. Proc Inst Mech Eng I: J Syst Control Eng 226(2):175–187. https://doi.org/10.1177/0959651811414507
12. Lee N, Kamamichi N, Li H, Furuta K (2008) Control system design and experimental verification of capsubot. In: Proc. of IEEE/RSJ int. conf. on intelligent robotics and systems, Nice, France, pp 22–26
13. Yu H, Hude MH, Wane SO (2011) A novel acceleration profile for the motion control of capsubots. In: Proc. of IEEE int. conf. on robotics and automation, Shanghai, China, pp 2437–2442
14. Zhang C, Tan R, Liu H, Li H (2013) Control strategy of vibrational capsubot in viscoelastic environment. Engineering 5:424–428. https://doi.org/10.4236/eng.2013.510B087
15. Mahmoudzadeh S, Mojallali H (2015) An optimized motion strategy for the legless capsubot using non-linear optimization. J Control Eng Appl Inf 17(4):81–89
16. Lee N, Kamamichi N, Ishikawa J, Furuta K (2009) Positioning control of a capsule robot using sliding mode control. In: Proc. of IEEE int. conf. on robotics and biomedics, Guillin, China, pp 995–1000
17. Mahmoudzadeh S, Mojallali H, Purjafari N (2014) An optimized PID for capsubots using modified chaotic genetic algorithm. Int J Eng Trans. C 27:1377–1384
18. Huda MN, Yu H (2015) Trajectory tracking control of an underactuated capsubot. Auton Robots 39:183–198. https://doi.org/10.1007/s10514-015-9434-3
19. Huda MN, Yu H, Cang S (2015) Behaviour-based control approach for the trajectory tracking of an underactuated planar capsule robot. IET Control Theory Appl 9(2):163. https://doi.org/10.1049/iet-cta.2013.1100
20. Chen W, Fang M, Yu H (2009) Model predictive control applied into time delay capsubot system. In: Proc. of international conference on intelligent human-machine systems and cybernetics, pp 112–115. https://doi.org/10.1109/IHMSC.2009.36
21. Sume PA, Babiarz A (2021) On control of a capsubot robot. In: Proc. of 25th international conference on methods and models in automation and robotics, pp 390–394. https://doi.org/10.1109/MMAR49549.2021.9528465
22. Liu Y, Yu H, Yang TC (2008) Analysis and control of a capsubot. In: Proc. of IFAC congress, Seoul, Korea, pp 756–761
23. Liu Y, Wiercigroch M, Pavlovskaia E, Yu H (2013) Modelling of a vibro-impact capsule system. Int J Mech Sci 66:2–11. https://doi.org/10.1016/j.ijmecsci.2012.09.012
24. Ivanov AP (2019) On the optimization of a capsubot with a spring. In: VIII international conference on computational methods for coupled problems in science and engineering, pp 213–220
25. Nguyen VD, La NT (2020) An improvement of vibration-driven locomotion module for capsule robots. Mech Based Des Struct Mach. https://doi.org/10.1080/15397734.2020.1760880
26. Whittaker ET (1970) A Treatise on the analytical dynamics of particles and rigid bodies. Cambridge University Press, Cambridge
27. Suzuki Y, Li H, Furuta K (2007) Locomotion generation of friction board with an inclined slider. In: Proc. of IEEE conf. decision and control, New Orleans, USA, pp 1937–1943
28. Figurina T, Grlazkov T (2020) Optimization of the rectilinear motion of a capsule system along a rough plane. ZAMM J Appl Math Mech. https://doi.org/10.1002/zamm.202000111

29. Su G, Zhang C, Tan R, Li H (2009) A design of the electromagnetic driver for the "internal force-static friction" capsubot. In: Proc. of IEEE/RSJ international conference on intelligent robots and systems, pp 613–617. https://doi.org/10.1109/IROS.2009.5354587
30. Blajar W (1992) A projection method approach to constraint dynamic analysis. J Appl Mech 59:643–649
31. Furuta K (2002) Super mechano systems: fusion of control and mechanism. In: Plenary of 15th IFAC world congress, Barcelona, Spain, pp 35–44
32. Furuta K, Ohata A, Sugiki A, Saito M (2009) Discrete adaptive control of mechanism. In: Plenary Address of int. multiconference, control theory and systems, Moscow, Russia, pp 171–179